Applied Surface Science 499 (2020) 143913

Contents lists available at ScienceDirect

Applied Surface Science

journal homepage: www.elsevier.com/locate/apsusc

Full length article

Impact of germanium substrate orientation on morphological and structural properties of graphene grown by CVD method

Jakub Sitek[a,*], Iwona Pasternak[a], Justyna Grzonka[b,1], Jan Sobieski[a], Jaroslaw Judek[a], Pawel Dabrowski[c], Mariusz Zdrojek[a], Wlodek Strupinski[a]

[a] Faculty of Physics, Warsaw University of Technology, Koszykowa 75, 00-662 Warsaw, Poland
[b] Faculty of Engineering and Materials Science, Warsaw University of Technology, Woloska 141, 02-507 Warsaw, Poland
[c] Faculty of Physics and Applied Informatics, University of Lodz, Pomorska 149/153, 90-236 Lodz, Poland

ARTICLE INFO

Keywords:
Graphene
Germanium
CVD
Crystallographic orientation
Surface reconstruction
Raman spectroscopy

ABSTRACT

In this paper we study graphene synthesized on undoped (001), (110), and (111) Ge substrates, and show how the surface orientation and reconstruction affect its morphological and structural properties. The article presents the first attempt to explain the impact of germanium surface reconstruction on the shape and the density of graphene nuclei as well as on the material's stress and doping levels. Our findings suggest that graphene obtained on Ge(001) is the most uniform, with low doping ($1.5 \times 10^{12}\,cm^{-2}$) and low strain level ($-0.1\%$). Graphene on Ge(110) appears to be highly compressed (-0.5%) while graphene on Ge(111) exhibits doping reaching $5 \times 10^{13}\,cm^{-2}$. These results help to better understand the dynamics of graphene growth on germanium and indicate Ge(001), in terms of its structural properties, as the most promising orientation for the future CMOS applications.

1. Introduction

Since its isolation in 2004 [1], graphene has captured the attention of the scientific community worldwide. Its remarkable properties, such as carrier mobility reaching up to $350{,}000\,cm^2\,V^{-1}\,s^{-1}$ and high optical transparency (97.7%), make it a viable candidate for the electronics industry [2,3]. However, to effectively realize the application potential of this 2D material, high quality and large-scale graphene synthesis is required. To date, several techniques to produce graphene have been developed, such as mechanical exfoliation, chemical intercalation, and recently described pulsed-laser scribing [1,4,5]. But the most common method to synthesize high-quality single-layer graphene is chemical vapor deposition (CVD) [6]. It can be used to grow graphene on a variety of surfaces, including SiC, Cu, Ni, hBN, Pt or Ir [6–11], which, however, have their own set of advantages and drawbacks. It was revealed that the substrate type strongly affects the structural, morphological, and electronic properties of graphene. The material's parameters are altered not only by the surface's chemical composition, but also by its polytype, polar face, crystallographic orientation, and miscut [12,13]. The charge carrier density in graphene fabricated on 4H-SiC, for example, differs distinctly from graphene on 6H-SiC [14]. In GR/Cu systems Cu(111) plane promotes graphene with a lower number of layers compared to other orientations [15]. Additionally, it was shown that crystal orientation has larger impact on the defect density compared to the facet roughness [16]. But the biggest challenge in growing graphene on metal surfaces is the fact that it involves a necessary transfer step, which imposes various constraints related to graphene impurities and defects. In addition, the automation difficulties practically make it impossible to integrate this graphene technology with Si CMOS (complementary metal-oxide-semiconductor) production. Hence, the research focus was shifted toward the search for better alternatives.

In 2013 copper was attended to be replaced with CMOS-compatible germanium [17], thus, allowing graphene to be grown directly as part of the electronic circuit. The in-situ growth also helps to overcome issues related to the impurities formed during the graphene transfer [18]. The substrate-graphene dependencies, however, remain a challenge [19]. The initial investigation revealed the impact of Ge orientation on graphene properties and its growth mechanism. Graphene can be synthesized on three main orientations of germanium monocrystals: Ge (001), Ge(110), and Ge(111), as well as on their epitaxial equivalents, i.e. Ge(001)/Si(001), Ge(110)/Si(110), and Ge(111)/Si(111), both commercially available. Graphene can be grown on all indicated surfaces by methods such as CVD [17,19–24], MBE [25], PVD [26], and

* Corresponding author.
E-mail address: jakub.sitek@pw.edu.pl (J. Sitek).
[1] Current address: INL – International Iberian Nanotechnology Laboratory, Av. Mestre José Veiga, 4715-330 Braga, Portugal.

https://doi.org/10.1016/j.apsusc.2019.143913
Received 27 May 2019; Received in revised form 30 July 2019; Accepted 8 September 2019
Available online 09 September 2019
0169-4332/

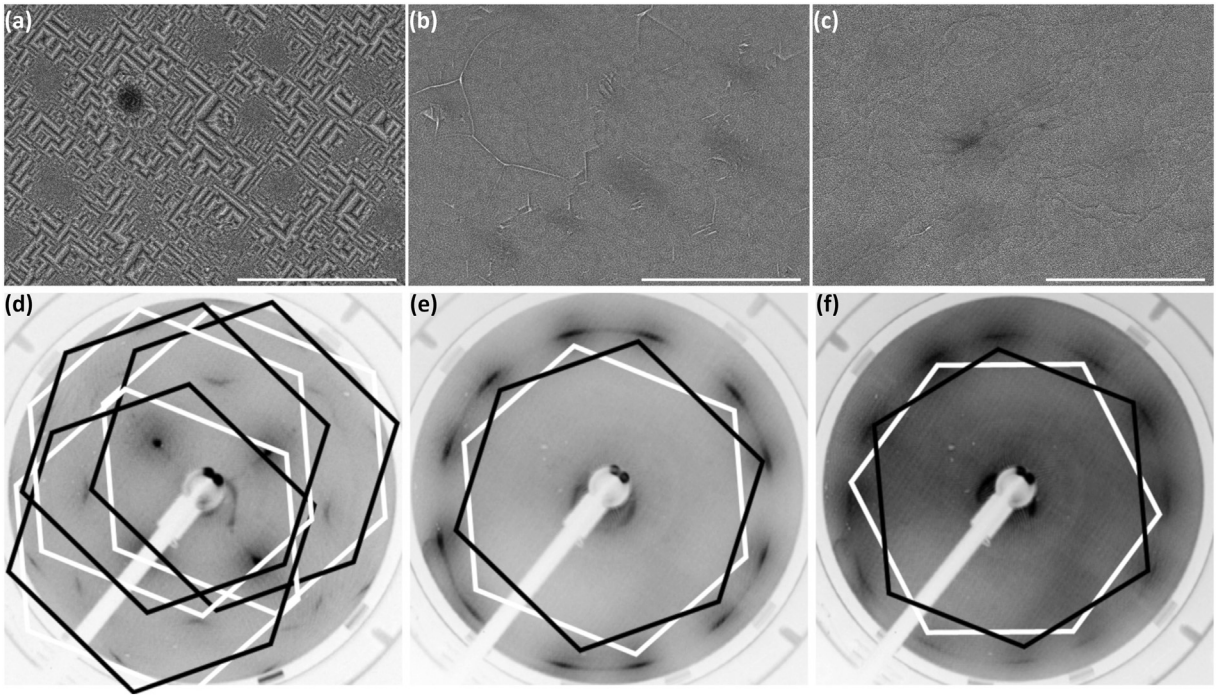

Fig. 1. SEM images of the morphology of continuous graphene layer and the underlying substrate on: (a) Ge(001); (b) Ge(110); (c) Ge(111). Scale bars are 1 μm. LEED measurements recorded at 75 eV for: (d) Ge(001); (e) Ge(110); (f) Ge(111).

electron beam evaporation [27], which also affects the quality of graphene layers. Furthermore, there are clear differences in the topography features and electronic properties of graphene depending on crystal orientation of germanium substrate. One of the first works on this subject [19], based on Raman spectroscopy, STM, and XPS, shows a variance in doping and strains in graphene grown on differently oriented Ge substrates. In addition to the inherent variations of graphene properties related to the initial germanium orientation, after in situ annealing at 700 °C, Kiraly et al. observed further strain modification driven by the Ge surface reconstruction [19]. It is also noted that graphene on Ge(001), despite being the most technologically relevant, exhibits the highest stress level. This finding is reported in papers of Tesch and Pham [20,27], highlighting that GR/Ge interfaces in Ge(110) and Ge(111) are flatter than in Ge(001), with reduced topography roughness. It must be noted, however, that Kiraly obtained graphene synthesized on bulk Ge(001), Ge(110), and Ge(111) with variable doping and resistivity. This may cause the substrate-dopant segregation at the GR/Ge interface, and, in consequence, negatively impact the study conclusions. STM and LEED measurements, on which further studies were focused, are valuable, however, they are limited to a restricted area. The optimization of the graphene technology requires a more statistically-oriented characterization of surfaces, enabling better assessment of the overall graphene quality. There is also a need to further study graphene grown on Ge substrates with identical doping, and to research how graphene grows on different germanium orientations.

In this work, we present the analysis of the graphene growth mechanism as well as the morphological, structural, and electronic properties of the layers grown on (001), (110), and (111) oriented germanium substrates. In order to study the growth kinetics, we characterized graphene at the initial growth step prior to graphene domains merger, which enabled us to establish coverage area, nucleation density, and domain size. Raman characterization of the continuous graphene layer unveils strain and doping levels depending on the germanium orientation. The further sections discuss the influence of surface reconstruction on these parameters. Our results are an important step toward understanding the germanium substrate influence on graphene, and pave the way for the future integration of graphene in the CMOS technology.

2. Experimental section

2.1. Sample preparation

Graphene was grown by the CVD method on undoped Ge(001), Ge (110), and Ge(111) wafers supplied by Semiconductor Wafer Inc. Growth runs were performed in commercially available Aixtron G5 WW CVD system equipped with the planetary reactor, which enabled us to achieve high uniformity of graphene films over the whole area of the 15 × 15 mm substrates. As described in our previous works [21,22], we sustained the growth at the temperature of 905 °C in an Ar/CH_4 mixture at 800 mbar. As a cleaning procedure, directly before the growth we annealed the substrates at 905 °C in hydrogen flow sustained at 500 SCCM for 15 min. The growths were performed in two ways. Firstly, we achieved a continuous layer by extending the time to 3 h. Secondly, in order to determine graphene nuclei density, the graphene growth was stopped before the graphene domains started to merge (1 h). All three orientations were used in each growth run.

2.2. Graphene characterization

The surface morphology of the as-grown samples was investigated by a high-resolution SEM Hitachi SU8230 Cold-FEG equipped with a semi-in-lens type objective lens. The observations were performed simultaneously in a low voltage range at 0.5 kV to obtain topographic information and in deceleration mode to improve resolution. Further microscopy studies consisted of AFM measurements, conducted in a non-contact mode in Bruker FastScan AFM microscope. The low-energy electron diffraction (LEED) measurements were performed at room temperature (RT) under the base pressure of 2×10^{-10} mbar in Multiprobe P system made by Omicron GmbH (currently known as Scienta-Omicron). Raman spectroscopy investigations were realized by a Renishaw inVia system with a 532 nm Nd:YAG laser as an excitation source to obtain single-point and spatially distributed Raman spectra.

Graphene coverage area, nucleation density, and domain size were estimated by an ImageJ software.

3. Results and discussion

The process which resulted in the formation of a continuous graphene layer allowed us to investigate the Ge surface morphology modified after the growth, and to check the quality of graphene in terms of the presence of wrinkles and voids. The micrographs of graphene on three orientations are presented in Fig. 1a–c. For Ge(001) characteristic [107] facets occurred (Fig. 1a), reported previously [28]. On Ge(110) graphene wrinkles are present, yet they do not extend to any particular direction (Fig. 1b). The underlying substrate did not undergo evident surface changes, contrary to Ge(111) where a high density of terraces and steps is visible (Fig. 1c). Furthermore, graphene layer grown on Ge(111) does not exhibit wrinkling.

Additionally to SEM images, LEED patterns were acquired for Ge (001), Ge(110), and Ge(111) (Fig. 1d–f). The results indicate the presence of crystalline graphene domains on all germanium orientations. Graphene grown on Ge(001) has two planar graphene domain orientations marked with black and white hexagons. However, due to the presence of germanium nanofacets, we also observed different domain orientations. These orientations are visible as three pairs of hexagons and the explanation of their origin was presented in detail earlier [21,29].

In case of Ge(110) and Ge(111) there are two main domain directions of graphene relative to the germanium substrate. The absence of different directions relative to the LEED spectrometer indicates that the substrate is smooth and lacks nanofacets. Nonetheless, the LEED pattern obtained for graphene/Ge(111) is significantly blurred due to the graphene-germanium interaction. These results are consistent with our previous work in which we showed that the interaction between graphene and germanium increases for flat germanium substrates [29]. Hence, we expect the weakest interaction between graphene and Ge (001).

To further investigate the graphene-germanium interface, we conducted AFM studies of the continuous layer (Fig. 2). The image of GR/Ge(001) shows the formation of germanium nanofacets on the entire surface (Fig. 2a), as well as confirms lack of oxidation of the underlying Ge substrate [30]. The average height of nanofacets is in the range of a few nanometers. However, graphene on Ge(001) is not visible as it does not form wrinkles, and other defects are not present. In case of Ge(110), graphene can be easily distinguished from the underlying substrate (Fig. 2b). The graphene wrinkles are much more pronounced (approx. 5 nm) than the atomic steps of germanium substrate (approx. 0.6 nm), which was observed in the previous studies [20]. The atomic steps, due to their low height, are difficult to observe in the topography contrast during SEM examination. The third substrate, Ge(111), exhibits intriguing surface reliefs, similar to the terraces and steps seen in the SEM micrograph (Fig. 2c). The height of the surface features lies between the height of Ge(001) nanofacets and atomic steps of Ge(110) and ranges from 0.7 to 1 nm. More interestingly, the height of the features seems to be changing continuously, in contrast to Ge(110), where a clear difference between individual atomic steps can be seen. On all three samples a height profile has been made and the resulting height plots are shown in Fig. 2d.

When germanium is fully covered with graphene, however, we are not able to gather direct and easily accessible information on graphene domain shapes, nucleation density, growth rate, and domain size. Therefore, we shortened the graphene growth process. The summary of nucleation density, graphene coverage area (as a measure of the growth rate), and domain size is presented in Table 1. Most domains ($2.00 \times 10^6\,mm^{-2}$), of the average size of 500 × 500 nm, are grown on Ge(001) and also the coverage area is the highest, i.e. 29%. On the contrary, the lowest nucleation density ($1.36 \times 10^6\,mm^{-2}$) and the lowest coverage area (18%) can be observed on Ge(110) and Ge(111), respectively. The lower coverage area of graphene on Ge(110) and Ge (111) results from the lower growth rate, which, in turn, enables better process control. Also, if the nucleation density on both Ge(110) and Ge (111) is decreased compared to Ge(001), there are fewer grain boundaries, which due to pseudo-Hall-Petch effect could increase elastic modulus of graphene and lead to lower strain levels [31]. Interestingly, the growth time of the shortened process was one-third of the time required to achieve a continuous layer, so we expected the coverage area to be at least 33%, but for all three orientations this value is evidently smaller. We suggest that carbon atoms are attached to the

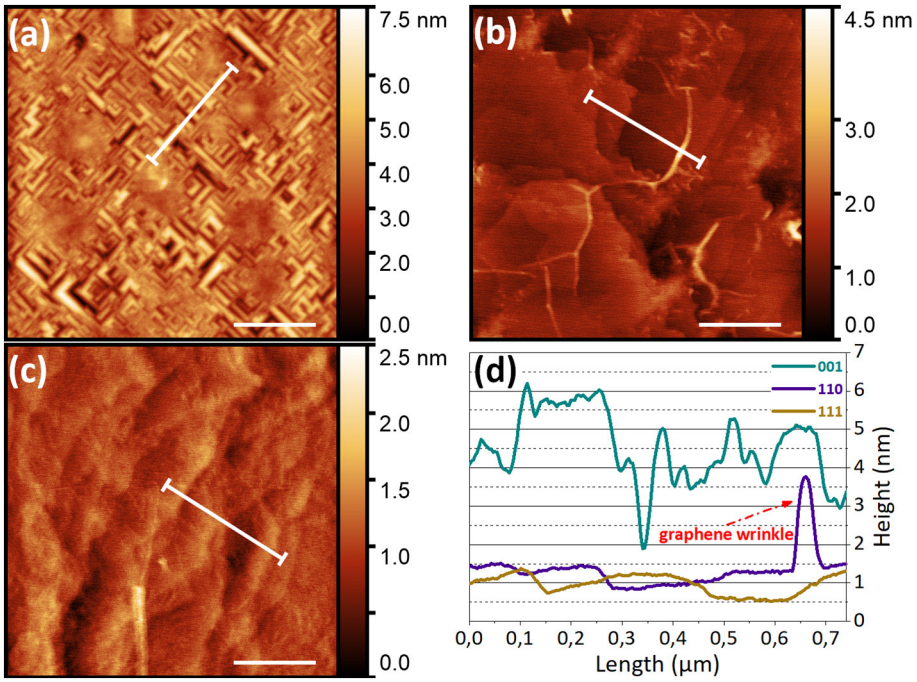

Fig. 2. AFM images of: (a) Ge(001); (b) Ge(110); (c) Ge(111); and (d) graph showing height profiles of the samples. The profiles are marked on the AFM images. Scale bars are 500 nm.

Table 1
Nucleation density, coverage area, and average domain dimensions of graphene on different orientations.

Ge orientation	Nucleation density [$10^6 \times mm^{-2}$]	Coverage area [%]	Average domain dimensions [nm × nm]
(001)	2.00	29	500 × 500
(110)	1.36	22	930 × 315
(111)	1.65	18	490 × 350

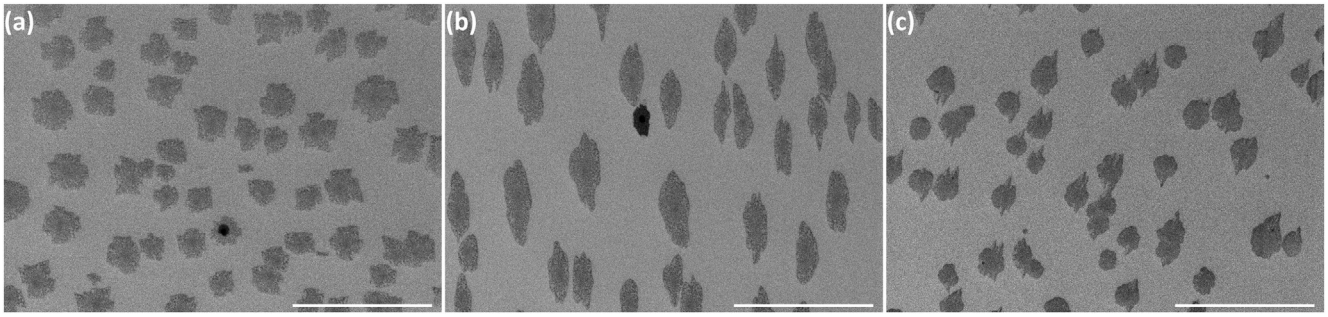

Fig. 3. SEM images of graphene domains on: (a) Ge(001); (b) Ge(110); (c) Ge(111). Scale bars are 2 μm.

edges of nuclei, therefore as the domains grow larger and the boundary length is increased, the growth rate accelerates. As shown in Fig. 3, the substrate orientation impacts the growth process, and consequently the shapes of domains and their arrangement. On Ge(001) there is no preferred nuclei "spread" direction, which might be connected with several graphene domain orientations, and graphene islands propagate isotropically. In contrast, both on Ge(110) and Ge(111) the growth is anisotropic and the shape of the graphene islands on Ge(110) is clearly elongated (Fig. 3b). Furthermore, on Ge(110) all domains are aligned along [−110], which agrees well with the results of Dai et al. [32].

An interesting phenomenon occurs on Ge(111) where atomic steps of germanium can be seen (Fig. 4). The presence of the steps could be explained by the unintentional miscut of the substrate. We can observe how graphene moves along the atomic steps, with the nuclei's core, however, remaining circular and proliferating on terraces, resembling step-flow growth present in III-V compounds epitaxy [33]. Atomic steps, and, in general, any pits and hillocks on the substrate surface, are energetically favorable nucleation sites for the graphene growth [34]. After coalescence of the domains, the alignment of the atomic steps changed, creating a more random network with one direction manifesting stronger (Fig. 4b).

Nevertheless, some observations could not be clearly understood or interpreted. For example, nucleation density should be lower on Ge (001) where the surface should have least defects and/or atomic steps. As faceting is the result of the graphene growth, it cannot explain the phenomenon of nucleation sites formation [28]. Another phenomenon, which can impact the growth of graphene on Ge, is surface reconstruction. As the germanium orientations (001), (110), or (111) undergo reversible surface reconstruction at elevated temperatures, the initial arrangement of atoms obviously changes at the growth temperature of 905 °C. This phenomenon was investigated superficially and only at a low temperature [19,20,26,27,29,35,36].

We introduce the first analysis of the impact of germanium surface reconstruction at the growth temperature on graphene properties. The surface reconstruction of Ge(001) changes from (2 × 1) at RT to a regular (1 × 1) structure at 682 °C, with probable melting at even higher temperatures. As the surface reconstruction is minuscule (the atoms are moving closer to each other), the number of surface atoms remains the same [37–39]. Ge(110) is not very different, with c(8 × 10) at RT and, by intermediate subtle shifts, partially reconstructed again to an elongated c(8 × 10) at 837 °C, also with incomplete melting [40–42]. Finally, Ge(111) undergoes reconstruction from c(2 × 8) at RT through (1 × 1) at 297 °C to a regular $(1 \times 1)_h$ at 777 °C, changing the surface energy due to a different number of surface atoms. Ge(111) reconstruction appears most pronounced, as one-third of the restatoms are overlaid by the adatoms during cooling, significantly modifying the surface energy [43]. This reconstruction is also similarly described as incomplete melting [43,44]. In particular, the incomplete melting

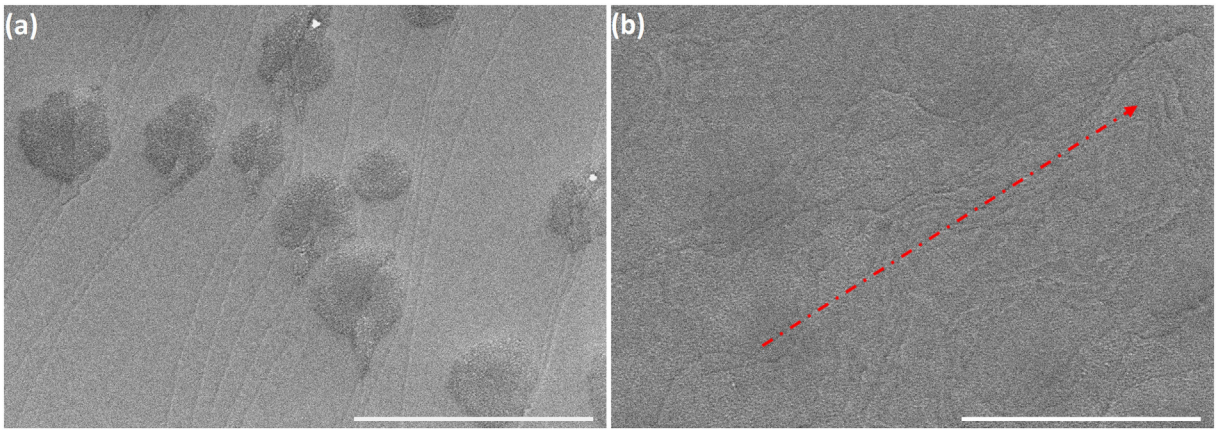

Fig. 4. High-magnification (×50 k) SEM images of: (a) graphene nuclei on Ge(111); (b) network of atomic steps on Ge(111). The red dashed arrow indicates the main direction of atomic steps. Scale bars are 1 μm. The samples were differently rotated during SEM characterization.

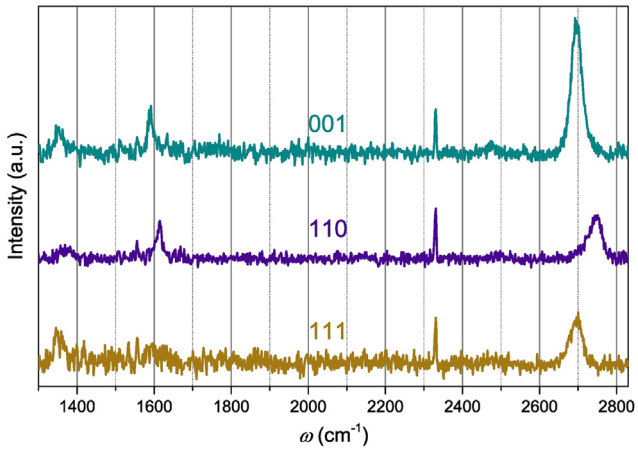

Fig. 5. Raman spectra of graphene on Ge(001), Ge(110) and Ge(111). The narrow peak near 2330 cm^{-1} is attributed to ambient nitrogen. The spectra are normalized to the nitrogen peak.

affects only the first bilayer of germanium, which has been reported only for Ge(111) [44], while it should apply to other orientations. For all three orientations at the growth temperature, the surface is exhibiting metallic behavior, resulting from the overlap of electronic bands. There is no connection between the surface reconstruction and faceting on Ge(001) as the former involves only several atomic layers and the latter much thicker volume of germanium.

We can conclude that previously presented growth mechanisms should be considered deficient since surface reconstruction is not included. Surface reconstruction and incomplete surface melting would definitely have an impact on the graphene growth. One clear difference in the surface reconstruction is between Ge(110) and both Ge(001) and Ge(111), where, at the growth temperature, the first exhibits more complex c(8 × 10) structure than (1 × 1) on (001) and (111). Apart from the unreconstructed restatom arrangement, this could also help to interpret the similar nuclei shape on (001) and (111) and different on (110).

To further examine the graphene-germanium interactions, we conducted Raman characterization. The representative Raman spectra of graphene on all three orientations are presented in Fig. 5. A distinct and narrow 2D peak is visible on all orientations, nevertheless, its position (denoted as ω_{2D}) and intensity is varying significantly between different substrates. The variation of peak position and intensity is as well observed for G peak. D peak is present on all orientations, however, as it is shown in the literature, the presence of D peak, especially on Ge(111), seems to be an inherent property of the GR/Ge system [23]. A peak near 2330 cm^{-1} is attributed to ambient nitrogen.

The variation of ω_G and ω_{2D} clearly indicates differences between Ge orientations which can be attributed to strain and/or doping levels of the graphene layer. To investigate this, we analyzed the ω_{2D}-ω_G correlation according to Lee et al. [45], which allowed us to quantitatively assess the stress and the doping (Fig. 6a). For the reference point, we used ω_G = 1581.6 cm^{-1} and ω_{2D} = 2676.9 cm^{-1} of the suspended graphene, and for the reference strain and doping lines we used $\Delta\omega_{2D}/\Delta\omega_G$ = 2.23 and $\Delta\omega_{2D}/\Delta\omega_G$ = 0.55, respectively [46,47]. As it can be seen, there is no significant dispersion of peak positions in Ge(001), where the strain is slightly compressive (−0.1%) and the hole doping is almost negligible (between 0 and 5 × 10^{12} cm^{-2}). In case of Ge(110), the stress is more intense and reaches up to −0.5%, which is the highest value of all orientations, with virtually no doping. The 2D position of Ge(111), in contrast, is fixed at approx. 2695 cm^{-1} while G moves significantly in the range between 1595 and 1620 cm^{-1}, which is similar to Ge(110). The hole doping is varied, in some areas well exceeding 1.5 × 10^{13} cm^{-2}. These results stand in contradiction with experimental data presented by Kiraly et al. who showed behavior similar to that observed in Ge(110). This discrepancy might be caused by the fact that the group used doped and undoped substrates, which could have interfered with graphene properties. They also stated that graphene on Ge(001) is the most stressed while our Raman and LEED findings suggest the opposite.

Graphene on Ge(001) is low strained and doped, with the narrowest dispersion of all the orientations. This observation can be confirmed with SEM images, and can be linked to the shape of nuclei and surface reconstruction of the substrate. The domain shape on Ge(001) is regular, driven by the low surface reconstruction of (1 × 1), changing at RT only slightly to (2 × 1), therefore we expected a low strain level.

For Ge(111), the correlation between ω_{2D} and ω_G shown in the graph in Fig. 6a is not straightforward. One explanation of the fixed ω_{2D} is that doping compensates strain in graphene, resulting in lower stresses for highly doped regions. Another hypothesis can be linked to the step network, visible in the SEM images. The interpretation is that graphene grows along atomic steps, to which it is strongly attached by covalent bonds, as suggested by Dai et al. [32]. On terraces graphene edges are terminated by hydrogen and the layer is attached by van der Waals forces, hence manifesting less stringent bonding to the substrate. During cooling, when surface reconstructs back from (1 × 1) to c (2 × 8) and there is a change in the atomic steps network, the graphene layer can behave differently on terraces and steps, leading to expansion and contraction in perpendicular directions, i.e. zig-zag and armchair, according to Poisson effect, as a result nearly completely cancelling out the strain. This hypothesis is supported by LEED measurements which show blurred graphene spots, indicating a complex graphene-substrate interaction. Interestingly, this quasi-random atomic step network is present only on Ge(111), while on Ge(001) nanofacets are visible and Ge(110) is nearly flat (Fig. 1, Fig. 2). Since $\Delta\omega_{2D}/\Delta\omega_G$ for armchair and zig-zag directions differs and equals 2.44 and 2.02 [45], respectively, there could be sets of strains that result in a fixed ω_{2D} and shifts in ω_G caused by the doping. The doping, simultaneously, can be an effect of the surface reconstruction, as at the RT two-thirds of the atoms which were in the direct contact with the graphene, moved deeper modifying the electronic states of graphene. This mechanism can be described as an electrostatic doping, probably workfunction-induced, contrastingly to spontaneous polarization typical for various SiC polytypes [14,48,49]. This hypothesis, to some extent, could also explain the difference between our work and Kiraly's since the surface of germanium substrates may differ.

Fig. 6b shows the plot of 2D peak width (full width at half maximum, Γ_{2D}) against Γ_G. The dispersion of data points of GR/Ge(001) is low, indicating a high-quality graphene [50]. Graphene grown on Ge (111) behaves differently, with a wide distribution of Γ_G, revealing less uniform layer. Nonetheless, both samples are exhibiting similar behavior, i.e. roughly constant Γ_{2D} and variable Γ_G. The most interesting, though, is the alignment of the data from graphene on Ge(110), which are ordering along the line with a slope equaling 1.76. This value is slightly lower than that reported by Neumann and Shin (2.2–2.3) [46,50], however, it suggests that the strain variations are in the nanometer-scale, within the size of a laser spot. As discussed earlier, this might be an effect of the different, compared to Ge(001) and Ge(111), surface reconstruction.

The strain (ε)-doping (n_h) dependence is shown in Fig. 6c. The results in this graph can be estimated more accurately than in Fig. 6a, therefore, the scale-exceeding doping level of graphene on Ge(111) can be assessed as high as 5 × 10^{13} cm^{-2}. The data points related to graphene grown on (001) and (111) are following a similar trend as in Fig. 6b, exhibiting a linear dependency. On the contrary, the results of the strain-doping correlation for graphene deposited on Ge(110) are widely spread, not following any particular direction. We can conclude that there is the same cause at the supra-atomic level in case of Ge(001) and Ge(111) as in Fig. 6b, which, again, can be attributed to the surface reconstruction.

Histograms in Fig. 6d are depicting the quality of the graphene

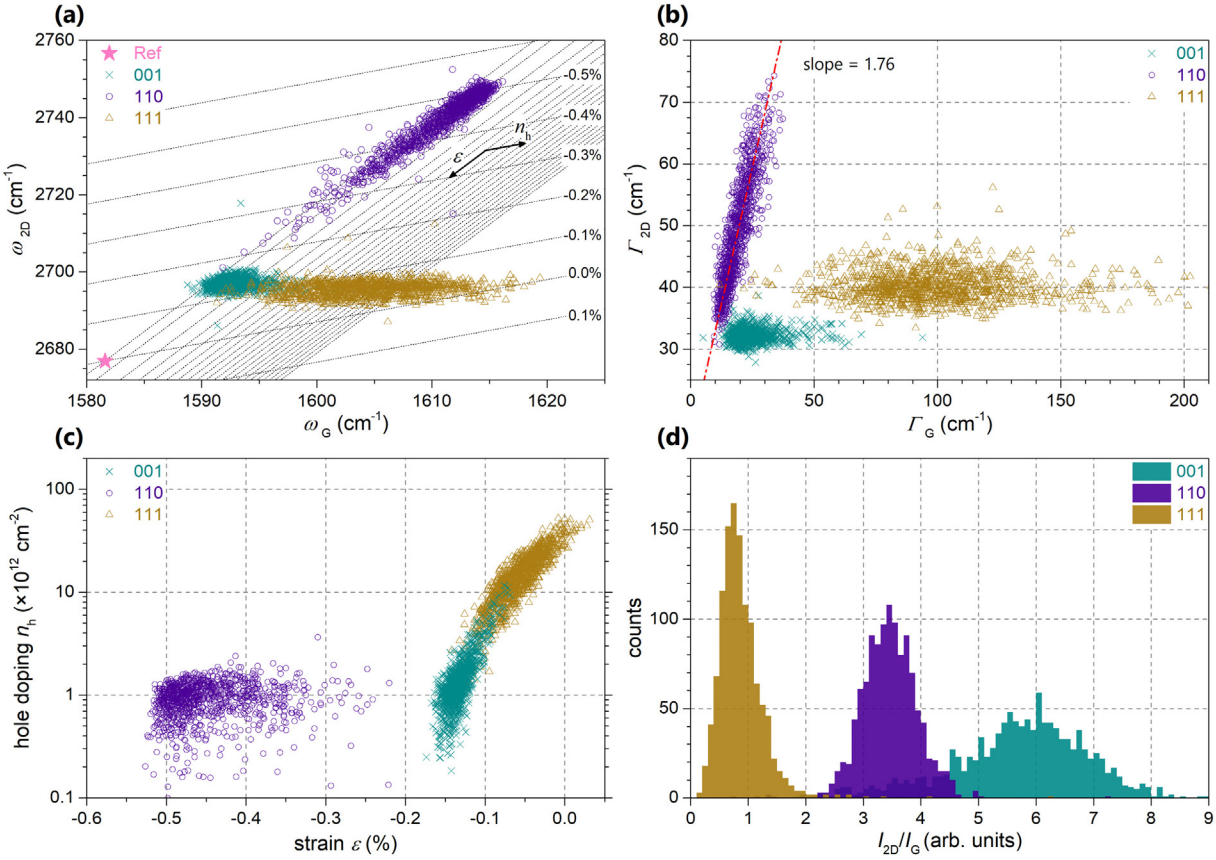

Fig. 6. Different dependencies between graphene grown on three orientations: (a) correlation between ω_{2D} and ω_G; the doping lines are separated by the value of 1×10^{12} cm^{-2}; (b) correlation between Γ_{2D} and Γ_G; (c) correlation between hole doping (n_h) and strain (ε); (d) histogram of the ratio I_{2D}/I_G.

layer, expressed in terms of I_{2D}/I_G ratio [51]. Ge(001) represents the highest quality of all three orientations, resulting from low Γ_G as well as intense 2D peak. On the contrary, the lowest average I_{2D}/I_G (below 1) is exhibited for (111), caused by a very broad G peak. The quality of graphene obtained on Ge(110) is at the mid-range level (I_{2D}/I_G = 3.5).

Whereas the positions of Raman G and 2D modes can provide information on carrier concentration and strain acting on graphene, the intensities of the D and G modes can be used for calculation of the mean distance between structural defects L_D and their concentration n_D. The model proposed in Ref [52–54], which according to the authors should be valid for a wide class of point defects that are Raman active, provides following equations:

$$L_D^2(\mathrm{nm}^2) = \frac{4300}{E_L^4}\left(\frac{I_D}{I_G}\right)^{-1},$$

$$n_D(\mathrm{cm}^{-2}) = 7.3{\bullet}10^9{\bullet}E_L^4\left(\frac{I_D}{I_G}\right),$$

where E_L stands for energy of the laser line used for excitation. Histograms of distribution of L_D and n_D are shown in Fig. 7a. As can be seen, the most defected graphene was grown on Ge(001), despite the fact that this substrate is characterized by the largest I_{2D}/I_G ratio, which is often treaded as another quality parameter. The less defected graphene was grown on Ge(110) substrate, despite the large strain value and an average value of the I_{2D}/I_G ratio. Graphene grown on Ge(111) substrate is characterized by the largest spread of values of L_D and the lowest I_{2D}/I_G value. We note that obtained defects concentration values are not expected to correlate with the hole doping levels shown in Fig. 7b since these are different quantities.

4. Conclusion

In this report, we investigated graphene grown on undoped Ge substrates with three different orientations, namely (001), (110), and (111), and suggested the connection between germanium surface reconstruction at the growth temperature, graphene nuclei shape, and the strain levels. Graphene domains on Ge(001) are circular, however, on Ge(110) are distinctly elongated, and on Ge(111) are following the atomic steps. We determined that the lowest nucleation density is on Ge (111), while Ge(001) yields the highest coverage area. Raman studies revealed different electrostatic doping and stress in all three orientations, showing that graphene on Ge(001) exhibits low doping and strain levels with the lowest dispersion of data. Additionally, we suggest that the graphene growth mechanism is affected by the germanium surface reconstruction, which could explain why graphene on Ge(110) is the most stressed, as well as the reason for the fixed ω_{2D} and the doping level of GR/Ge(111). We can conclude that graphene fabricated on Ge (001), despite the highest nucleation density and the presence of [107] facets, is the most uniform due to the smallest surface reconstruction, which will be advantageous for the future application of graphene in the CMOS technology.

Acknowledgements

The authors acknowledge the support by the European Union Graphene Flagship funding (Grant Graphene Core2 n° 785219). This work was supported by the National Science Centre, Poland, nr UMO-2016/23/D/ST5/00633. The authors would also like to thank Nano Carbon sp. z o.o. for the use of their CVD reactor and Raman spectroscope.

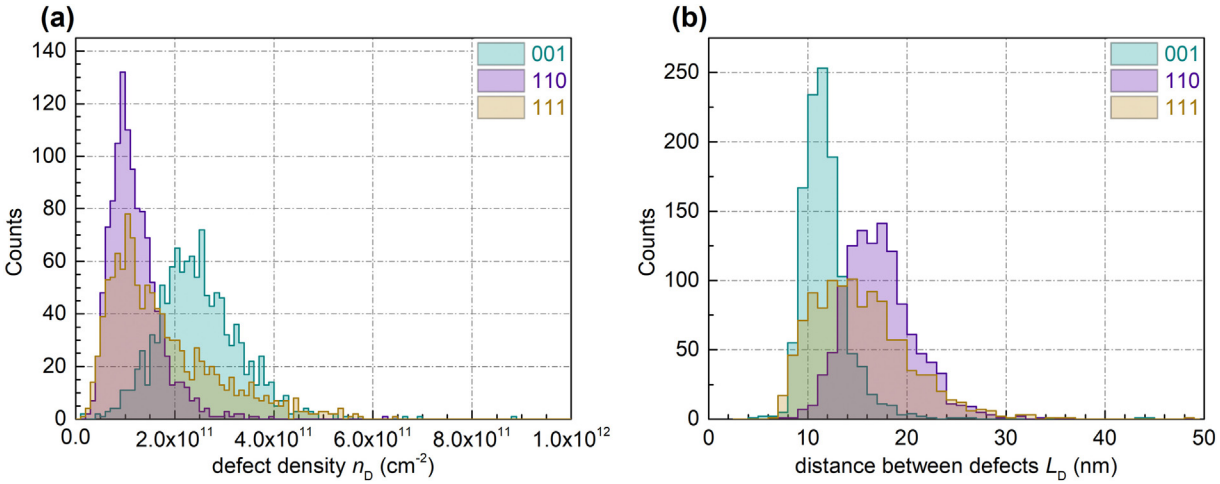

Fig. 7. (a) Calculated defect density on different germanium orientations; (b) calculated distance between defects on different germanium orientations.

Declaration of competing interests

The authors declare no competing financial interest.

References

[1] K.S. Novoselov, A.K. Geim, S.V. Morozov, D. Jiang, Y. Zhang, S.V. Dubonos, I.V. Grigorieva, A.A. Firsov, Electric field in atomically thin carbon films, Science 306 (2004) 666–669, https://doi.org/10.1126/science.1102896.

[2] L. Banszerus, M. Schmitz, S. Engels, J. Dauber, M. Oellers, F. Haupt, K. Watanabe, T. Taniguchi, B. Beschoten, C. Stampfer, Ultrahigh-mobility graphene devices from chemical vapor deposition on reusable copper, Sci. Adv. 1 (2015) 1–6, https://doi.org/10.1126/sciadv.1500222.

[3] R.R. Nair, P. Blake, A.N. Grigorenko, K.S. Novoselov, T.J. Booth, T. Stauber, N.M.R. Peres, A.K. Geim, Fine structure constant defines visual transparency of graphene, Science 320 (2008) 1308, https://doi.org/10.1126/science.1156965.

[4] M.J. McAllister, J.L. Li, D.H. Adamson, H.C. Schniepp, A.A. Abdala, J. Liu, M. Herrera-Alonso, D.L. Milius, R. Car, R.K. Prud'homme, I.A. Aksay, Single sheet functionalized graphene by oxidation and thermal expansion of graphite, Chem. Mater. 19 (2007) 4396–4404, https://doi.org/10.1021/cm0630800.

[5] Y. Chyan, R. Ye, Y. Li, S.P. Singh, C.J. Arnusch, J.M. Tour, Laser-induced graphene by multiple lasing: toward electronics on cloth, paper, and food, ACS Nano 12 (2018) 2176–2183, https://doi.org/10.1021/acsnano.7b08539.

[6] X. Li, W. Cai, J. An, S. Kim, J. Nah, D. Yang, R. Piner, A. Velamakanni, I. Jung, E. Tutuc, S.K. Banerjee, L. Colombo, R.S. Ruoff, Large area synthesis of high quality and uniform graphene films on copper foils, Science 324 (2009) 1312–1314, https://doi.org/10.1126/science.1171245.

[7] W. Strupinski, K. Grodecki, A. Wysmolek, R. Stepniewski, T. Szkopek, P.E. Gaskell, A. Grüneis, D. Haberer, R. Bozek, J. Krupka, J.M. Baranowski, Graphene epitaxy by chemical vapor deposition on SiC, Nano Lett. 11 (2011) 1786–1791, https://doi.org/10.1021/nl200390e.

[8] A. Reina, X. Jia, J. Ho, D. Nezich, H. Son, V. Bulovic, M.S. Dresselhaus, K. Jing, Large area, few-layer graphene films on arbitrary substrates by chemical vapor deposition, Nano Lett. 9 (2009) 30–35, https://doi.org/10.1021/nl801827v.

[9] S. Tang, H. Wang, Y. Zhang, A. Li, H. Xie, X. Liu, L. Liu, T. Li, F. Huang, X. Xie, M. Jiang, Precisely aligned graphene grown on hexagonal boron nitride by catalyst free chemical vapor deposition, Sci. Rep. 3 (2013) 1–7, https://doi.org/10.1038/srep02666.

[10] T.A. Land, T. Michely, R.J. Behm, J.C. Hemminger, G. Comsa, STM investigation of single layer graphite structures produced on Pt(111) by hydrocarbon decomposition, Surf. Sci. 264 (1992) 261–270, https://doi.org/10.1016/0039-6028(92)90183-7.

[11] J. Coraux, A.T. N'Diaye, C. Busse, T. Michely, Structural coherency of graphene on Ir(111), Nano Lett. 8 (2008) 565–570, https://doi.org/10.1021/nl0728874.

[12] G. Yazdi, T. Iakimov, R. Yakimova, Epitaxial graphene on SiC: a review of growth and characterization, Crystals 6 (2016) 53, https://doi.org/10.3390/cryst6050053.

[13] C. Virojanadara, R. Yakimova, J.R. Osiecki, M. Syväjärvi, R.I.G. Uhrberg, L.I. Johansson, A.A. Zakharov, Substrate orientation: a way towards higher quality monolayer graphene growth on 6H-SiC(0001), Surf. Sci. 603 (2009) L87–L90, https://doi.org/10.1016/j.susc.2009.05.005.

[14] T. Ciuk, P. Caban, W. Strupinski, Charge carrier concentration and offset voltage in quasi-free-standing monolayer chemical vapor deposition graphene on SiC, Carbon 101 (2016) 431–438, https://doi.org/10.1016/j.carbon.2016.01.093.

[15] A.T. Murdock, A. Koos, T.B. Britton, L. Houben, T. Batten, T. Zhang, A.J. Wilkinson, R.E. Dunin-Borkowski, C.E. Lekka, N. Grobert, Controlling the orientation, edge geometry, and thickness of chemical vapor deposition graphene, ACS Nano 7 (2013) 1351–1359, https://doi.org/10.1021/nn3049297.

[16] J.D. Wood, S.W. Schmucker, A.S. Lyons, E. Pop, J.W. Lyding, Effects of polycrystalline Cu substrate on graphene growth by chemical vapor deposition, Nano Lett. 11 (2011) 4547–4554, https://doi.org/10.1021/nl201566c.

[17] G. Wang, M. Zhang, Y. Zhu, G. Ding, D. Jiang, Q. Guo, S. Liu, X. Xie, P.K. Chu, Z. Di, X. Wang, Direct growth of graphene film on germanium substrate, Sci. Rep. 3 (2013) 1–6, https://doi.org/10.1038/srep02465.

[18] A. Ambrosi, M. Pumera, The CVD graphene transfer procedure introduces metallic impurities which alter the graphene electrochemical properties, Nanoscale 6 (2014) 472–476, https://doi.org/10.1039/C3NR05230C.

[19] B. Kiraly, R.M. Jacobberger, A.J. Mannix, G.P. Campbell, M.J. Bedzyk, M.S. Arnold, M.C. Hersam, N.P. Guisinger, Electronic and mechanical properties of graphene–germanium interfaces grown by chemical vapor deposition, Nano Lett. 15 (2015) 7414–7420, https://doi.org/10.1021/acs.nanolett.5b02833.

[20] J. Tesch, E. Voloshina, M. Fonin, Y. Dedkov, Growth and electronic structure of graphene on semiconducting Ge(110), Carbon 122 (2017) 428–433, https://doi.org/10.1016/j.carbon.2017.06.079.

[21] I. Pasternak, P. Dabrowski, P. Ciepielewski, V. Kolkovsky, Z. Klusek, J.M. Baranowski, W. Strupinski, Large-area high-quality graphene on Ge(001)/Si (001) substrates, Nanoscale 8 (2016) 11241–11247, https://doi.org/10.1039/C6NR01329E.

[22] I. Pasternak, M. Wesolowski, I. Jozwik, M. Lukosius, G. Lupina, P. Dabrowski, J.M. Baranowski, W. Strupinski, Graphene growth on Ge(100)/Si(100) substrates by CVD method, Sci. Rep. 6 (2016) 21773, , https://doi.org/10.1038/srep21773.

[23] J.-H. Lee, E.K. Lee, W.-J. Joo, Y. Jang, B.-S. Kim, J.Y. Lim, S.-H. Choi, S.J. Ahn, J.R. Ahn, M.-H. Park, C.-W. Yang, B.L. Choi, S.-W. Hwang, D. Whang, Wafer-scale growth of single-crystal monolayer graphene on reusable hydrogen-terminated germanium, Science 344 (2014) 286–289, https://doi.org/10.1126/science.1252268.

[24] A.M. Scaparro, V. Miseikis, C. Coletti, A. Notargiacomo, M. Pea, M. De Seta, L. Di Gaspare, Investigating the CVD synthesis of graphene on Ge(100): toward layer-by-layer growth, ACS Appl. Mater. Interfaces 8 (2016) 33083–33090, https://doi.org/10.1021/acsami.6b11701.

[25] G. Lippert, J. Dąbrowski, T. Schroeder, M.A. Schubert, Y. Yamamoto, F. Herziger, J. Maultzsch, J. Baringhaus, C. Tegenkamp, M.C. Asensio, J. Avila, G. Lupina, Graphene grown on Ge(001) from atomic source, Carbon 75 (2014) 104–112, https://doi.org/10.1016/j.carbon.2014.03.042.

[26] P.C. Rogge, M.E. Foster, J.M. Wofford, K.F. McCarty, N.C. Bartelt, O.D. Dubon, On the rotational alignment of graphene domains grown on Ge(110) and Ge(111), MRS Commun. 5 (2015) 539–546, https://doi.org/10.1557/mrc.2015.63.

[27] T.T. Pham, N.D. Nam, R. Sporken, Surface morphology, structural and electronic properties of graphene on Ge(111) via direct deposition of solid-state carbon atoms, Thin Solid Films 639 (2017) 84–90, https://doi.org/10.1016/j.tsf.2017.08.031.

[28] K.M. McElhinny, R.M. Jacobberger, A.J. Zaug, M.S. Arnold, P.G. Evans, Graphene-induced Ge (001) surface faceting, Surf. Sci. 647 (2015) 90–95, https://doi.org/10.1016/j.susc.2015.12.035.

[29] P. Dabrowski, M. Rogala, I. Pasternak, J. Baranowski, W. Strupinski, M. Kopciuszynski, R. Zdyb, M. Jalochowski, I. Lutsyk, Z. Klusek, The study of the interactions between graphene and Ge(001)/Si(001), Nano Res. 10 (2017) 3648–3661, https://doi.org/10.1007/s12274-017-1575-6.

[30] P. Dabrowski, M. Rogala, I. Pasternak, P. Krukowski, J.M. Baranowski, W. Strupinski, I. Lutsyk, D.A. Kowalczyk, S. Pawłowski, Z. Klusek, Early oxidation stages of germanium substrate in the graphene/Ge(001) system, Carbon 149 (2019) 290–296, https://doi.org/10.1016/j.carbon.2019.04.036.

[31] Z. Song, V.I. Artyukhov, B.I. Yakobson, Z. Xu, Pseudo Hall–Petch strength reduction in polycrystalline graphene, Nano Lett. 13 (2013) 1829–1833, https://doi.org/10.1021/nl400542n.

[32] J. Dai, D. Wang, M. Zhang, T. Niu, A. Li, M. Ye, S. Qiao, G. Ding, X. Xie, Y. Wang, P.K. Chu, Q. Yuan, Z. Di, X. Wang, F. Ding, B.I. Yakobson, How graphene islands are unidirectionally aligned on the Ge(110) surface, Nano Lett. 16 (2016) 3160–3165, https://doi.org/10.1021/acs.nanolett.6b00486.

[33] Y. Horikoshi, H. Yamaguchi, F. Briones, M. Kawashima, Growth process of III-V

compound semiconductors by migration-enhanced epitaxy, J. Cryst. Growth 105 (1990) 326–338, https://doi.org/10.1016/0022-0248(90)90382-U.
[34] W. Liu, H. Li, C. Xu, Y. Khatami, K. Banerjee, Synthesis of high-quality monolayer and bilayer graphene on copper using chemical vapor deposition, Carbon 49 (2011) 4122–4130, https://doi.org/10.1016/j.carbon.2011.05.047.
[35] J. Tesch, F. Paschke, M. Fonin, M. Wietstruk, S. Böttcher, R.J. Koch, A. Bostwick, C. Jozwiak, E. Rotenberg, A. Makarova, B. Paulus, E. Voloshina, Y. Dedkov, The graphene/n-Ge(110) interface: structure, doping, and electronic properties, Nanoscale 10 (2018) 6088–6098, https://doi.org/10.1039/C8NR00053K.
[36] J. Grzonka, I. Pasternak, P.P. Michałowski, V. Kolkovsky, W. Strupinski, Influence of hydrogen intercalation on graphene/Ge(0 0 1)/Si(0 0 1) interface, Appl. Surf. Sci. 447 (2018) 582–586, https://doi.org/10.1016/j.apsusc.2018.04.029.
[37] K. Terakura, T. Yamasaki, Y. Morikawa, Structural phase transition on Si(001) and Ge(001) surfaces, Phase Transit. 53 (1995) 143–163, https://doi.org/10.1080/01411599508200394.
[38] A. Santoni, V.R. Dhanak, Electronic structure of the high-temperature Ge(1 0 0) surface studied by valence band photoemission, Surf. Sci. 537 (2003) L423–L428, https://doi.org/10.1016/S0039-6028(03)00693-9.
[39] A.D. Laine, M. DeSeta, C. Cepek, S. Vandré, A. Goldoni, N. Franco, J. Avila, M.C. Asensio, M. Sancrotti, Surface phase transitions of Ge(100) from temperature-dependent valence-band photoemission, Phys. Rev. B 57 (1998) 14654–14657, https://doi.org/10.1103/PhysRevB.57.14654.
[40] X. Zeng, H.E. Elsayed-Ali, Time-resolved structural study of low-index surfaces of germanium near its bulk melting temperature, Phys. Rev. B: Condens. Matter Mater. Phys. 64 (2001) 085410, , https://doi.org/10.1103/PhysRevB.64.085410.
[41] A. Santoni, L. Petaccia, V.R. Dhanak, S. Modesti, High-temperature phase transitions at the Ge(110) surface, Surf. Sci. 444 (2000) 156–162, https://doi.org/10.1016/S0039-6028(99)01025-0.
[42] C.H. Mullet, S. Chiang, Reconstructions and phase transition of clean Ge(110), Surf. Sci. 621 (2014) 184–190, https://doi.org/10.1016/j.susc.2013.10.023.
[43] W. Mönch, Semiconductor Surfaces and Interfaces, 3rd ed., Springer Berlin Heidelberg, Berlin, Heidelberg, 2001, https://doi.org/10.1007/978-3-662-04459-9.
[44] N. Takeuchi, A. Selloni, E. Tosatti, Metallization and incomplete melting of a semiconductor surface at high temperature, Phys. Rev. Lett. 72 (1994) 2227–2230, https://doi.org/10.1103/PhysRevLett.72.2227.
[45] J.E. Lee, G. Ahn, J. Shim, Y.S. Lee, S. Ryu, Optical separation of mechanical strain from charge doping in graphene, Nat. Commun. 3 (2012) 1024–1028, https://doi.org/10.1038/ncomms2022.
[46] Y. Shin, M. Lozada-Hidalgo, J.L. Sambricio, I.V. Grigorieva, A.K. Geim, C. Casiraghi, Raman spectroscopy of highly pressurized graphene membranes, Appl. Phys. Lett. 108 (2016) 1–5, https://doi.org/10.1063/1.4952972.
[47] G. Froehlicher, S. Berciaud, Raman spectroscopy of electrochemically gated graphene transistors: geometrical capacitance, electron-phonon, electron-electron, and electron-defect scattering, Phys. Rev. B: Condens. Matter Mater. Phys. 91 (2015) 1–17, https://doi.org/10.1103/PhysRevB.91.205413.
[48] G. Gupta, B. Rajasekharan, R.J.E. Hueting, Electrostatic doping in semiconductor devices, IEEE Trans. Electron Devices 64 (2017) 3044–3055, https://doi.org/10.1109/TED.2017.2712761.
[49] M. Bokdam, P.A. Khomyakov, G. Brocks, Z. Zhong, P.J. Kelly, Electrostatic doping of graphene through ultrathin hexagonal boron nitride films, Nano Lett. 11 (2011) 4631–4635, https://doi.org/10.1021/nl202131q.
[50] C. Neumann, S. Reichardt, P. Venezuela, M. Drögeler, L. Banszerus, M. Schmitz, K. Watanabe, T. Taniguchi, F. Mauri, B. Beschoten, S.V. Rotkin, C. Stampfer, Raman spectroscopy as probe of nanometre-scale strain variations in graphene, Nat. Commun. 6 (2015) 8429, https://doi.org/10.1038/ncomms9429.
[51] J. Judek, I. Pasternak, P. Dabrowski, W. Strupinski, M. Zdrojek, Hydrogen intercalation of CVD graphene on germanium (001) – strain and doping analysis using Raman spectroscopy, Appl. Surf. Sci. 473 (2019) 203–208, https://doi.org/10.1016/j.apsusc.2018.12.104.
[52] M.Z. Iqbal, O. Kelekci, M.W. Iqbal, J. Eom, The structural and electrical evolution of chemical vapor deposition grown graphene by electron beam irradiation induced disorder, Carbon 59 (2013) 366–371, https://doi.org/10.1016/j.carbon.2013.03.030.
[53] A.C. Ferrari, J. Robertson, Interpretation of Raman spectra of disordered and amorphous carbon, Phys. Rev. B 61 (2000) 14095–14107, https://doi.org/10.1103/PhysRevB.61.14095.
[54] L.G. Cançado, A. Jorio, E.H.M. Ferreira, F. Stavale, C.A. Achete, R.B. Capaz, M.V.O. Moutinho, A. Lombardo, T.S. Kulmala, A.C. Ferrari, Quantifying defects in graphene via Raman spectroscopy at different excitation energies, Nano Lett. 11 (2011) 3190–3196, https://doi.org/10.1021/nl201432g.